ICAS 2021 SHANG HAI
International Council of the Aeronautical Sciences
32nd Congress of the International Council of the Aeronautical Sciences
September 6-10, 2021
Pudong Shangri-La, Shanghai, China

MATHEMATICAL MODELS FOR ANALYSIS AND OPTIMIZATION OF AIRCRAFT STRUCTURAL COMPONENTS TAKING INTO CONSIDERATION OF LOCAL STRESS DISTRIBUTION

V. Chedrik [1], S. Tuktarov [1], K. Balunov [1], N. Nguyen [2]

[1] Central Aerohydrodynamic Institute (TsAGI), Zhukovsky, Russia
[2] Moscow institute of physics and technology, Dolgoprudny, Russia

Abstract

Mathematical models for analysis and optimization problems of aircraft structural components concerning local stress distribution are presented. The numerical results of the structure made of both metallic and composite materials are discussed. Estimations of the influence of stresses in the chordwise direction on safety margins are given. The conclusions on applying known strength criteria at panel design with taking into account local stresses are done. The peculiarities for modeling a high-aspect-ratio composite wing using an anisotropic beam are highlighted. The problem concerning the determination of optimal shape plate in stress concentration zone, such as varying the plate thicknesses and hole geometry is of practical interest. Such a problem can be solved by using different optimization methods and mathematical models. The paper discusses the influence of mesh dimension, finite element types (2D/3D) on design parameters, and weight characteristics.

Keywords: finite element method, beam model, stress, wing-box, optimization

1. Introduction

In designing aircraft structures, peculiar attention is paid to the strength criteria for both regular and irregular parts. Observations at static tests show that structural failures generally occur in the stress concentration zones due to holes, stiffening elements, conjunctions, and so on. The study of stresses and strains in such zones is still an urgent problem nowadays. Mainly, it concerns the analysis of complex stress distribution in structures made of composite materials. There are the known classical solutions in the theory of elasticity for stress distribution in the hole zone [1, 2]. They give an understanding of stress distributions and their values at constant plate thickness. Nevertheless, when the thickness is non-uniform numerical methods should be used. The solution of the problem concerning the determination of optimal shape plate in stress concentration zone, such as varying the plate thicknesses and geometry of hole is of practical interest.

The presence of stiff ribs in modern aircraft wings provides the aerodynamic airfoils not to be deformed. However, it restrains the strains in the direction resulting in complex stress distribution in the vicinity of such stiffeners. The questions of elastic beam model development with anisotropic properties with/without deformations in the chordwise direction are outlined in paper [3]. Here, investigations of local stresses around cross stiffener are performed using finite element models of different fidelity levels to study the influence of local chordwise stresses on strength characteristics of optimum design. Some variants of numerical analysis are considered for the structure made of metallic and composite materials. Estimations of chordwise stress influence on strength margins are given. Some conclusions are proposed concerning the appliance of the strength criteria at panel design considering local stress distribution. Anisotropic beam modeling schemes for composite large aspect ratio wing are presented as effective in solving the optimization problems with taking into account strength and stiffness requirements.

2. Two approaches to modeling by anisotropic beam

Classical Bernoulli-Euler's beam theory is based on the following three kinematic assumptions:

- A cross-section is stiff in its surface.

- A cross-section remains plane with being deformed.
- A cross-section remains perpendicular to a deformed beam axis.

Experimental studies show that the assumptions are valid for long and thin beams made of isotropic material and having a solid section. If one or more of these conditions are violated, Bernoulli-Euler's beam theory can lead to inaccurate results. In the context of modeling of a medium- and high-aspect-ratio composite wing, there are three apparent differences from the ideal beam:

- the section is thin-walled and not solid;
- the wing-box skin and walls are made of a material having anisotropic characteristics;
- the wing-box width can be significantly larger than its height.

The placing of stiff ribs-diaphragms can guarantee to consider the wing-box section as stiff in its surface. Under beam theory assumptions, normal stresses in the section plane are considered negligible compared with normal stresses along the beam axis. This fact in Bernoulli-Euler's beam theory conflicts with the kinematic assumptions mentioned above. According to Hooke's law, linear deformations and normal stresses cannot be both equal to zero. At zero stresses, in-plane deformations should occur due to Poisson's effect.

On the contrary, zero deformations lead to non-zero normal stresses in the section plane. Further, two approaches to the beam model creation are given based on the general wing-box plate model. The first model is considered to have zero normal stresses along the lateral direction, and in the second model, the linear deformations are assumed to be zero. Within the mentioned above assumptions in the beam theory of isotropic body, we have two independent equations

$$M = EIv'', \quad T = GJ\theta',$$

where *M* and *T* are bending and torsional moments, *EI* and *GJ* – bending and torsional stiffnesses, v and θ – displacement along the *y*-axis and twist angle around the *z*-axis (Figure 1).

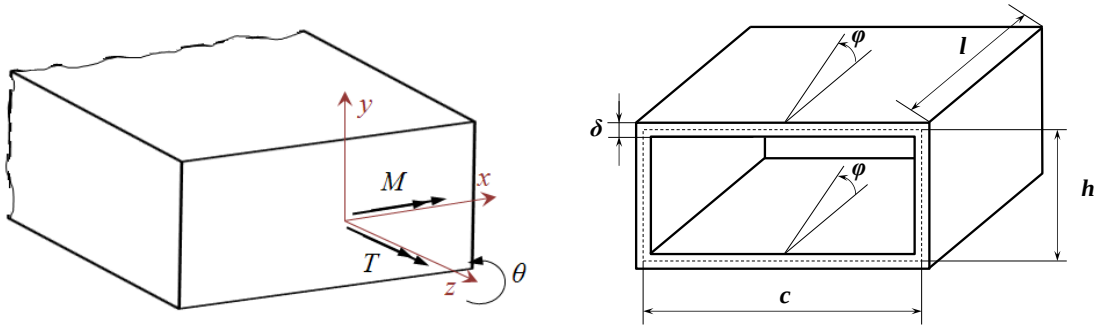

Figure 1 – Wing-box beam model: coordinate system, applied loads, geometry.

At the same time, in the presence of anisotropy, the relation between bend and torsion occurs [4, 5], expressed through the bending-torsional stiffness as

$$\begin{Bmatrix} M \\ T \end{Bmatrix} = \begin{bmatrix} EI & -K \\ -K & GJ \end{bmatrix} \begin{Bmatrix} v'' \\ \theta' \end{Bmatrix} \tag{1}$$

The solution of (1) is

$$\begin{Bmatrix} v'' \\ \theta' \end{Bmatrix} = \frac{1}{1-kg} \begin{bmatrix} 1/EI & g/EI \\ g/EI & 1/GJ \end{bmatrix} \begin{Bmatrix} M \\ T \end{Bmatrix},$$

where $k = K/EI$, $g = K/GJ$ and their product $\psi^2 = kg$ – so-called squared stiffness cross-coupling parameter. Using the solution, we define effective stiffnesses EI^* and GJ^* from the conditions of acting bending moment and torsion moment equal to zero, and vice versa, of acting torsion moment and bending moment equal to zero:

$$\frac{M}{v''} = EI(1-\psi^2) = EI^*, \qquad \frac{T}{\theta'} = GJ(1-\psi^2) = GJ^*.$$

From these ratios, the meaning of the parameter ψ can be seen: the higher is the degree of anisotropy, the less are the effective stiffnesses. Their maximum values are reached in the absence of anisotropy.

In order to determine the stiffnesses of composite wing-box, it is reasonable to utilize the laminated plate theory [6]. In this case, for the wing-box plate model, the ratios that link internal moments M_x, M_y, M_{xy} with curvatures $\kappa_x, \kappa_y, \kappa_{xy}$ through cylindrical stiffnesses D_{ij} in the analysis coordinate system of laminate (Figure 2) are written as

$$\begin{Bmatrix} M_x \\ M_y \\ M_{xy} \end{Bmatrix} = \begin{bmatrix} D_{11} & D_{12} & D_{16} \\ D_{12} & D_{22} & D_{26} \\ D_{16} & D_{26} & D_{66} \end{bmatrix} \begin{Bmatrix} \kappa_x \\ \kappa_y \\ \kappa_{xy} \end{Bmatrix} \tag{2}$$

According to classical laminated plate theory, the cylindrical stiffnesses D_{ij} for composite plate, containing *N* plies, are expressed through stiffness coefficients as:

$$D_{ij} = \frac{1}{3}\sum_{k=1}^{N} (\overline{Q}_{ij})_k (z_k^3 - z_{k-1}^3) \tag{3}$$

Stiffness coefficients $\overline{Q}_{ij}$ for separate *k*-th ply in the laminate system (Figure 2) are defined in terms of stiffness coefficients Q_{ij} in the ply system as follows:

$$\begin{aligned}
\overline{Q}_{11} &= Q_{11}\cos^4\varphi + 2(Q_{12} + 2Q_{66})\sin^2\varphi\cos^2\varphi + Q_{22}\sin^4\varphi \\
\overline{Q}_{12} &= (Q_{11} + Q_{22} - 4Q_{66})\sin^2\varphi\cos^2\varphi + Q_{12}(\sin^4\varphi + \cos^4\varphi) \\
\overline{Q}_{22} &= Q_{11}\sin^4\varphi + 2(Q_{12} + 2Q_{66})\sin^2\varphi\cos^2\varphi + Q_{22}\cos^4\varphi \\
\overline{Q}_{16} &= (Q_{11} - Q_{12} - 2Q_{66})\sin\varphi\cos^3\varphi + (Q_{12} - Q_{22} + 2Q_{66})\sin^3\varphi\cos\varphi \\
\overline{Q}_{26} &= (Q_{11} - Q_{12} - 2Q_{66})\sin^3\varphi\cos\varphi + (Q_{12} - Q_{22} + 2Q_{66})\sin\varphi\cos^3\varphi \\
\overline{Q}_{66} &= (Q_{11} + Q_{22} - 2Q_{12} - 2Q_{66})\sin^2\varphi\cos^2\varphi + Q_{66}(\sin^4\varphi + \cos^4\varphi)
\end{aligned} \tag{4}$$

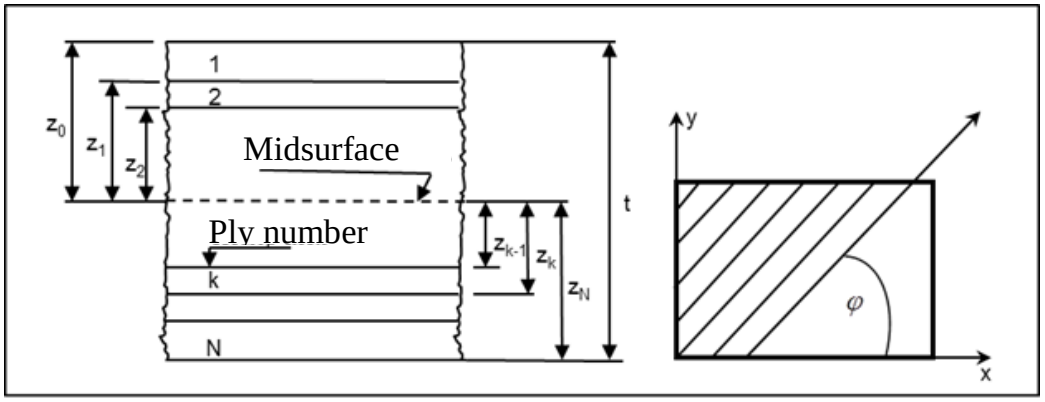

Figure 2 – The structure of the laminate.

According to Hooke's law in the case of orthotropic material, the stiffness coefficients for plies Q_{ij} can be found as functions of engineering material constants E_1, E_2, G_{12}, ν_{12}, ν_{21}:

$$Q_{11} = \frac{E_1}{1-\nu_{12}\nu_{21}},\ Q_{12} = \frac{\nu_{21}E_1}{1-\nu_{12}\nu_{21}},\ Q_{22} = \frac{E_2}{1-\nu_{12}\nu_{21}},\ Q_{66} = G_{12}, \tag{5}$$

where E_1 and E_2 are elastic modulus for lamina in two mutually perpendicular directions, G_{12} – shear modulus, ν_{12} and ν_{12} – Poisson's coefficients characterizing compression deformations along local ply axes 1 and 2 at tension along axes 2 and 1, correspondingly. For orthotropic ply, the condition $\nu_{21}E_1 = \nu_{12}E_2$ should be met as the elastic tensor is symmetric.

In further, all expressions will be considered in the global coordinate system (Figure 1). Reduced internal moments M_z and M_{xz} in this system are coupled with bending and torsional moments in beam section by formulas:

$$M = -M_z c,\ T = -2cM_{xz}.$$

The curvatures due to wing-box bending are expressed in terms of vertical displacement as follows:

$$\kappa_z = -\frac{\partial^2 v}{\partial z^2},\ \kappa_{xz} = -2\frac{\partial^2 v}{\partial x \partial z},\ \kappa_x = -\frac{\partial^2 v}{\partial x^2}.$$

We consider an example of bending of wing-box with orthotropic skin. The stiffness of walls is neglected. Internal moments arising from bending are given in terms of transverse displacement as:

$$M_x = -(D_x\frac{\partial^2 v}{\partial x^2} + D_1\frac{\partial^2 v}{\partial z^2}),\ M_z = -(D_z\frac{\partial^2 v}{\partial z^2} + D_1\frac{\partial^2 v}{\partial x^2}),\ M_{xz} = -2D_{xz}\frac{\partial^2 v}{\partial x \partial z},$$

where the cylindrical stiffnesses are defined by virtue of material characteristics $E_x, E_z, G_{xz}, \mu_{xz}$ and geometry parameters according to Eqs.(3)–(5) as follows:

$$D_x = \frac{E_x h^2 \delta}{2(1-\mu_{xz}\mu_{zx})},\quad D_z = \frac{E_z h^2 \delta}{2(1-\mu_{xz}\mu_{zx})},\quad D_{xz} = \frac{G_{xz} h^2 \delta}{2},\quad D_1 = \mu_{zx} D_x = \mu_{xz} D_z.$$

When only the bending moment is applied and the restraint deformations along the x-axis are assumed to be absent, we have $M_x = 0$. Therefore, the curvatures are related by the equation $\kappa_x = -\mu_{xz}\kappa_z$. Taking this, we can write the curvature κ_z through the bending moment $M = -cM_z$ similarly to beam elastic line equation as the Bernoulli–Euler's theory suggests:

$$\kappa_z = \frac{\partial^2 v}{\partial z^2} = \frac{M}{E_z I},\ \text{where}\ I = \frac{ch^2\delta}{2}. \tag{6}$$

At the presence of rigid transverse diaphragms in a wing-box modeled by an orthotropic plate, the deformations along the x-axis are strongly restrained so that the curvature κ_x can be neglected at bending, and it is assumed to be equal to 0. In this case, internal moments in the plate model are calculated as $M_x = -\mu_{xz} D_z \kappa_z$ and $M_z = -D_z \kappa_z$. Similarly to (6), the curvature κ_z and the transverse displacements can be found from the differential equation for a beam:

$$\kappa_z = \frac{\partial^2 v}{\partial z^2} = \frac{M(1-\mu_{xz}\mu_{zx})}{E_z I}. \tag{7}$$

The presence of restraint in the model also leads to normal stresses due to the internal moment $M_x = \mu_{xz} M_z$. Comparing (6) and (7), we can see that the ratio of wing displacement in this model to the similar one in the classical model is equal to $(1-\mu_{xz}\mu_{zx})$. Consider some special cases.

In the case of unstiffened aluminum skin (isotropic material) with Poisson's coefficient $\mu_{xz} = \mu = 0.3$, the stresses in the transverse direction in such beam model are about 30 % of normal stresses in the longitudinal direction, with the stresses signs being equal. At the same time, these stresses in Bernoulli-Euler's beam model are equal to 0. Obviously, in a real wing-box structure having rigid enough ribs the stresses in the transverse direction are not equal to 0. It is validated by further numerical analysis for the wing-box with isotropic skin. At design analyses of required thicknesses of wing skin, the equivalent stresses by von Mises criterion are used. In the absence of shift stresses, the equivalent stress in the model with restraint is lower by 11 % compared with the stress in the classical model, having zero stresses in the transverse direction. Such difference will decrease in the presence of shift stresses. From an engineering viewpoint, the classical model is preferable in this case as it gives underestimated safety margins in the skin, with the wing displacement being higher by 9 %.

For general stringer stiffened metallic skins (structural orthotropic panel), the equivalent characteristics for an orthotropic panel can be determined with the use of Eqs.(3)–(5). Consider the case of a panel with the reduced thickness twice larger than the skin thickness and made of aluminum alloy with mechanical characteristics $E = 72$ GPa, $\mu = 0.3$. Taking into account the fact that stringers in a panel work like rods, we have the following equivalent material characteristics: $E_z = 72$ GPa, $E_x = 37.7$ GPa, $\mu_{zx} = 0.3$, $\mu_{xz} = 0.157$, $G_{xz} = 13.8$ GPa. Here, in the absence of shift loads, the equivalent stress in the model with restraint in the chord direction is less by 6.9 % compared to the classical model, and the difference in displacements is equal to 4.7 %. In this case, at modeling the stiffened wing panel by orthotropic material, the resulting displacements and equivalent stresses regarding the restraint condition are highly close to real values. Note that at stiffening the panel by rigid ribs in the chord direction, the difference in results of the two models becomes less.

In general, for a composite wing, the Eq.(2) in a global coordinate system can be written as:

$$\begin{Bmatrix} -M/c \\ M_x \\ -T/(2c) \end{Bmatrix} = \begin{bmatrix} D_{22} & D_{12} & D_{26} \\ D_{12} & D_{11} & D_{16} \\ D_{26} & D_{16} & D_{66} \end{bmatrix} \begin{Bmatrix} -v'' \\ \kappa_x \\ 2\theta' \end{Bmatrix}. \quad (8)$$

The question arises how to reduce the system (8) containing three equations to the (1) having only two. In the first case, we neglect the chordwise normal stresses ($\sigma_x = 0$, i.e. $M_x = 0$). In the second case, obtaining the equations can be achieved assuming that the chordwise deformations in a wing-box skin are negligible ($\varepsilon_x = 0$) that corresponds to zero curvature κ_x at bending and meeting the general kinematic assumptions of Bernoulli-Euler's theory. Both of these cases have specific advantages at the structural analysis of a wing. Thus, for a narrow wing-box having low stiffness in the chordwise direction, it is reasonable to consider transverse normal stresses as 0. Nevertheless, if rigid ribs are located, in the case of composite wings having anisotropic material, it would be correct to suggest the chordwise deformations to be equal to 0 but transverse stresses not to be 0.

Further, we consider two beam models: model 1 is without restraint in the chord direction, model 2 is with chordwise restraint. For model 1, the Eq. (8) can be written as:

$$\begin{Bmatrix} M \\ T \end{Bmatrix} = c \begin{bmatrix} D_{22} - \dfrac{D_{12}^2}{D_{11}} & -2\left(D_{26} - \dfrac{D_{12}D_{16}}{D_{11}}\right) \\ -2\left(D_{26} - \dfrac{D_{12}D_{16}}{D_{11}}\right) & 4\left(D_{66} - \dfrac{D_{16}^2}{D_{11}}\right) \end{bmatrix} \begin{Bmatrix} y'' \\ \theta' \end{Bmatrix}.$$

Comparing Eq.(1), we obtain the expressions for stiffnesses of the wing-box beam model without restraint:

$$EI = c\left(D_{22} - \frac{D_{12}^2}{D_{11}}\right), \quad GJ = 4c\left(D_{66} - \frac{D_{16}^2}{D_{11}}\right), \quad K = 2\left(D_{26} - \frac{D_{12}D_{16}}{D_{11}}\right). \quad (9)$$

In assumptions of model 2, the Eq.(8) is reduced to

$$\begin{Bmatrix} M \\ T \end{Bmatrix} = c \begin{bmatrix} D_{22} & -2D_{26} \\ -2D_{26} & 4D_{66} \end{bmatrix} \begin{Bmatrix} y'' \\ \theta' \end{Bmatrix}.$$

For this model the stiffnesses are:

$$EI = cD_{22}, \quad GJ = 4cD_{66}, \quad K = 2D_{26}. \quad (10)$$

Note that the stiffnesses for model 2 are close to the ones for model 1 as the cylindrical stiffness D_{11} tends to infinity.

At the calculation of torsional stiffness, it is assumed that vertical spar webs carry shift stresses in both models. In Eq. (9) and (10), the webs are considered rigid since the plate analogy is used.

To calculate the torsional stiffness of thin-walled wing-box having one-closed contour and made of material with reduced shear modulus G, we apply Bredt's formula:

$$GJ = 4A^2 / \oint \frac{ds}{G\delta(s)},$$

where *A* is the contour square, the integral is taking along the middle line of the contour. For the wing-box given in Fig. 1, we have $GJ = 2c^2h^2G\delta/(c+h)$ taking into account of web's elasticity, and $GJ = 2G\delta ch^2$ considering rigid webs as in the case of the plate model. Specify the correction coefficient as the ratio of these torsional stiffnesses:

$$\gamma = (1 + h/c)^{-1}.$$

Further, the wing-box torsional stiffnesses will be considered as stiffnesses defined from Eq. (9) and (10) multiplied by the correction coefficient.

3. Composite wing-box example

As an example, we consider a thin-walled wing-box with a rectangular section, the length of which is l = 40 m, the width is c = 4 m and the height is d = 1 m. The skin and spar walls are made of composite material T3000 that has one unbalanced ply of thickness δ = 0.025 m with characteristics E_1 = 134 GPa, E_2 = 11 GPa, G_{12} = 7 GPa, ν_{12} = 0.22. The wing-box analysis is performed by use of two analytical models corresponding to the approaches described above. A ply orientation φ is varied

from 0° to 90° in both models. The same structure with corresponding ratios of geometric parameters and material characteristics were considered in [4]. The wing-box was fixed in a root section. In the first case, the resultant force of 10 kN was applied along the chord in the *y*-axis direction. In the second case, the torsion moment was idealized by two oppositely directed forces of 10^6 N, each was applied to the left and right spars of the tip section. The reduced values of effective bending $R_{EI} = EI^* / EI_0^*$ and torsion $R_{GJ} = GJ^* / GJ_0^*$ stiffnesses are shown in Fig. 3 for two models, where EI_0^* and GJ_0^* are composite wing-box stiffnesses for model 2 at the angle $\varphi = 0°$. The results are in good agreement with the ones obtained in the paper [4]. As it can be seen, two models are identical in bending stiffness and differ in torsion stiffness at the orientation of an unbalanced ply higher than 30°. For example, at the angle $\varphi = 60°$ the difference in torsion stiffnesses is more than twice. Thus, two models are close when the ply orientation is varied from 0° to 30°.

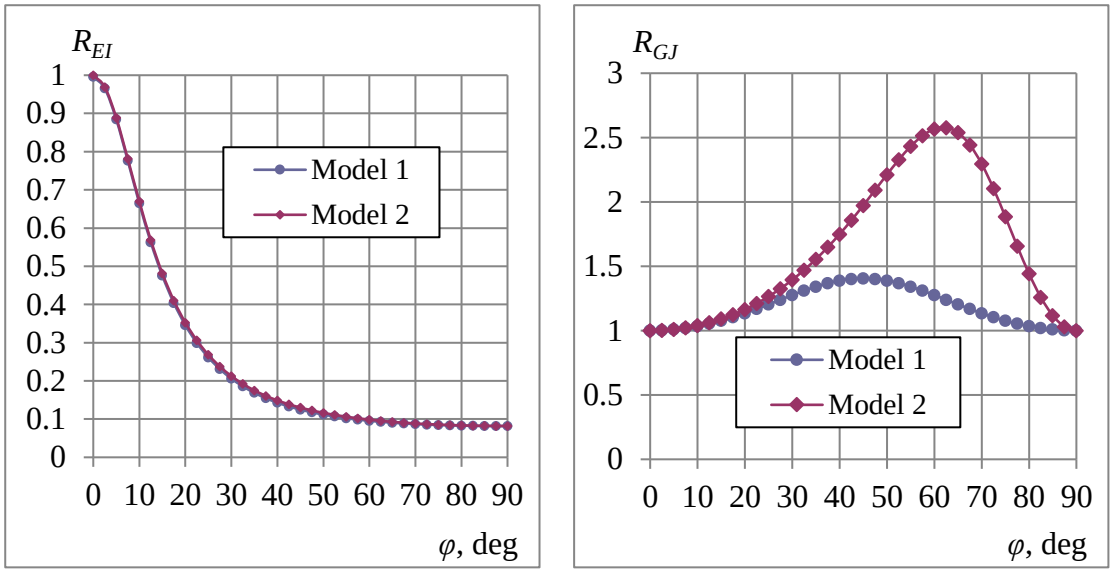

Figure 3 – The reduced bending (left) and torsion (right) stiffnesses for two beam models.

To verify the above analytical models, we create two finite element (FE) models of the anisotropic thin-walled wing-box. To exclude the restraint in the chord direction, we did not include ribs in the model 1 (Fig. 4, left). Furthermore, vice versa, stiff ribs in the model 2 provide near-zero deformations in the chord direction (Fig.4, right).

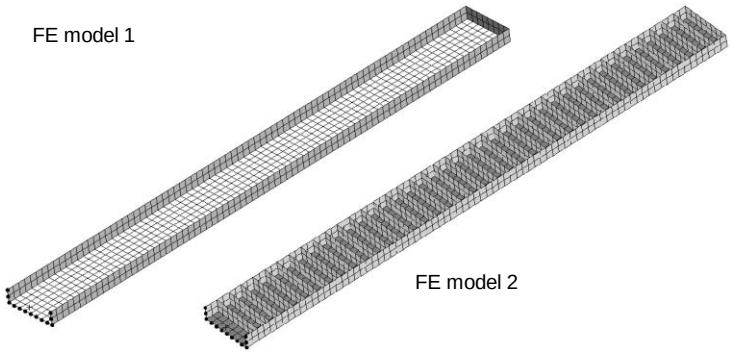

Figure 4 – FE models for two cases.

The material in walls has only shift characteristics to exclude their bending stiffness that was not taken into account in analytical models. Moreover, the shear modulus corresponds to the modulus of the laminate for each ply angle in the skin. The comparison of wing-box displacements is shown in Fig. 5 at bending, and of wing-box twist angles is presented in Fig. 6 at torsion moment.

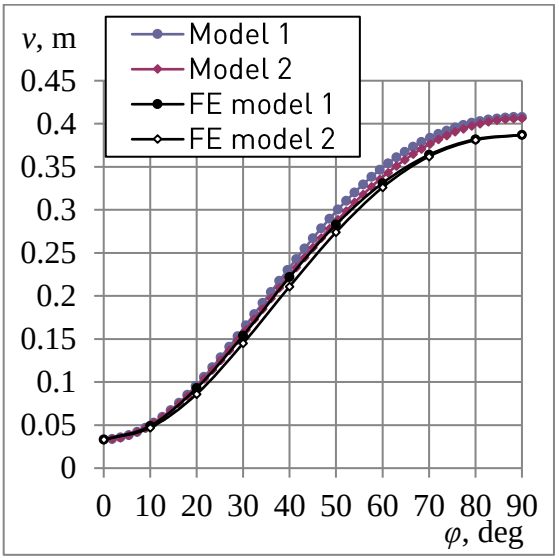

Figure 5 – Wing-box tip displacement at ply angle.

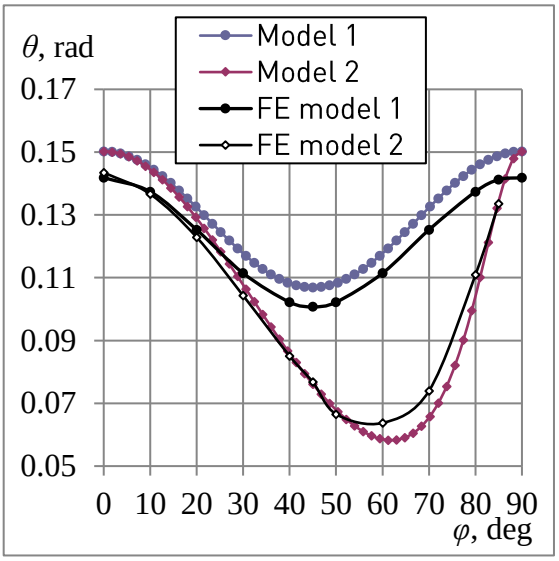

Figure 6 – Wing-box twist angle at ply angle.

Here, the analytical results are given for two models together with the corresponding to them FE results. As it can be seen, the results obtained by finite element analysis are in good agreement with the analytical ones for both models of the anisotropic beam. The difference in specified stiffness parameters does not exceed 5 %.

Based on FE stress analysis, the estimation of chordwise and equivalent stresses at the action of bending moment is performed for models 1 and 2 as well as for the model with ribs of typical stiff parameters ("realistic" model). In Fig. 7, the dependency of σ_x / σ_z from an unbalanced ply angle φ is shown for the point on the upper skin located at the distance of 4 m from the root section in the middle of the chord. It is seen that the results for the model 2 are in satisfactory agreement with the results for the 'realistic' model at low values of φ. Note that the maximum difference in results for the 'realistic' model comparing with models 1 and 2 is observed at the value of φ from 60° to 70°. Finite element analysis showed that the ratio σ_x / σ_z in the span direction at various values of φ is almost constant.

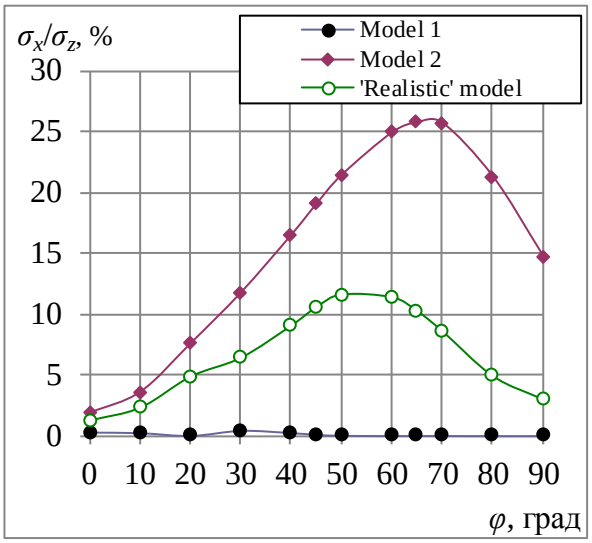

Figure 7 – The ratio of chordwise-to-spanwise stresses for three models.

Estimate the difference in equivalent stresses by von Mises for these three models at the angle of 60°. Assuming chordwise stresses $\sigma_x = 0$ in model 1, $\sigma_x = 0.25\sigma_z$ in model 2 and $\sigma_x = 0.12\sigma_z$ for model with typical cross stiffeners, we have the difference in equivalent stresses between beam models and the FE model with a typical set of stiffeners. As for model 1, the equivalent stresses are higher by 5.4 % and lower by 4.4 % in the model 2. Note that the equivalent stresses in both models are not significantly different even at the large distinction in chordwise normal stresses from the values corresponding to typical stiffnesses.

4. Stress and strength analysis of wing-box panels

At wing-box bending, its upper and lower panels are in the state of compression and tension, correspondingly. The relationship between the wing-box bending and torsion occurs due to the influence of linear deformations on shear stresses in a composite panel. Consider a three-section panel that is under acting tensile/compression load (Fig. 8).

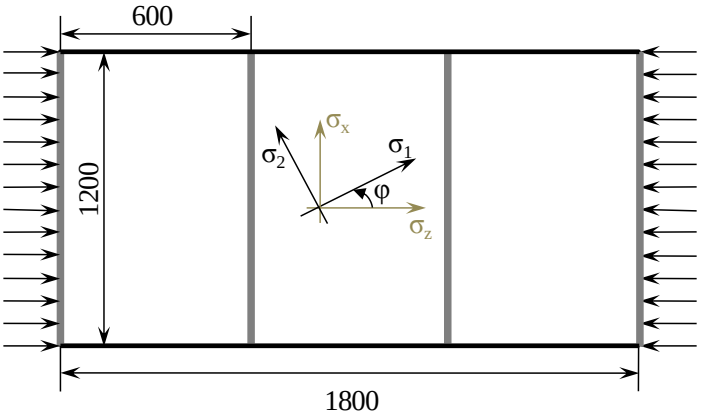

Figure 8 – Three-section panel (in mm).

Two cases are investigated: 1) the skin is made of aluminum material; 2) the skin is made of composite material KMU-7. The skin thickness is 5 mm. The spar/rib caps are modeled by beam elements with rectangular cross-sections. The section parameters for spars are taken as 160 mm and 5 mm, the least size for ribs was 5 mm and the second one was chosen from a set of 10, 20, 40, 80 and 160 mm. The composite layer has the next engineering characteristics: E_1 = 118 GPa, E_2 = 9.5 GPa, G_{12} = 5.9 GPa, ν_{12} = 0.36. Its strength is determined by allowable normal stresses in direction 1: $\bar{\sigma}_{1+}$ = 1540 MPa, $\bar{\sigma}_{1-}$ = 1210 MPa; in direction 2: $\bar{\sigma}_{2+}$ = 34 MPa, $\bar{\sigma}_{2-}$ = 200 MPa; allowable shear stresses $\bar{\tau}_{12}$ = 60 MPa. The laminate contains an unbalanced ply with the orientation angle varying from 0° to 90°. In the detailed FE model, the skin is modeled by square shell elements with a size of

20 mm, ribs and spars are represented by beam elements with bending stiffness. A distributed load P, the resultant value of which $2.4 \cdot 10^6$ N, is applied. Such load yields the normal spanwise stresses σ_z close to the allowable value of 400 MPa for aluminum alloy. In Fig. 9, the plots of spar chordwise displacements in the first wing-box bay are shown for various values of rib cross-sections.

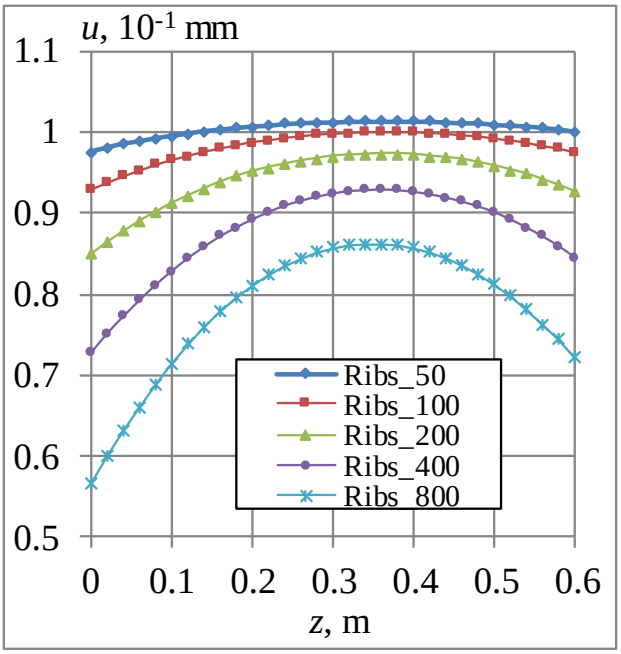

Figure 9 – Chordwise displacements.

As it can be seen, at the growth of cross-sections, the chordwise displacements decrease, and at the maximum value of the considered rib cross-sections, a strong restraint of deformations is observed, especially in rib-to-skin zones. Such fact results in sufficient stresses σ_x in the middle cross-section between ribs. The distribution of the stresses in the chord direction of the panel is shown in Fig. 10.

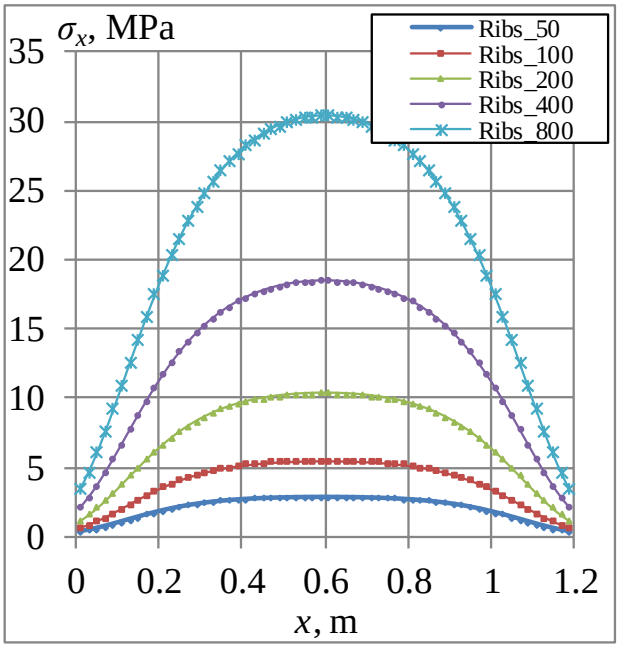

Figure 10 – Chordwise stresses.

Here the σ_x stresses reach the value of 8 % of spanwise stresses. The higher values (up to 12–15 %) are observed in the vicinity of rib caps (Fig. 11).

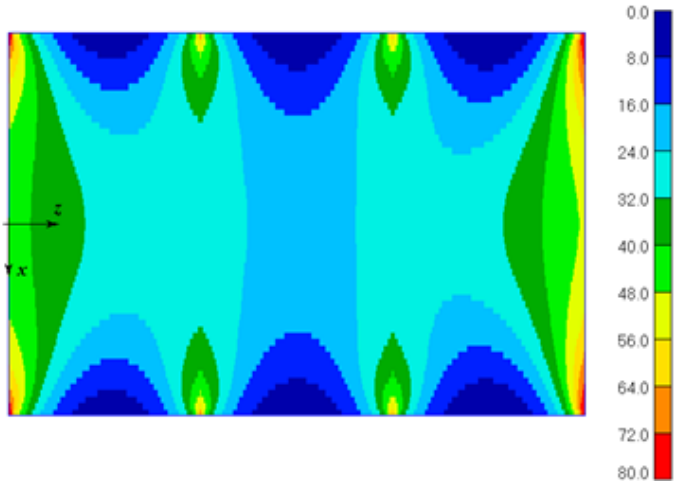

Figure 11 – The chordwise stress distribution (MPa).

Parametric analyses were performed to investigate the influence of the chordwise stiffness on the ratio $R_\sigma = \sigma_x / \sigma_z$ for a panel consisting of 9 bays. In Fig. 12, the dependencies of R_σ from r are shown for two zones, where r represents the ratio of the cross-section area of chordwise stiffeners to the product of the panel thickness and width. The upper curve corresponds to a central element on the skin near the rib (element 1 in Fig. 13), and the lower one corresponds to the center of the bay (element 2 in Fig. 13). The chordwise stresses in the panel are approximately 8.5–16 % of spanwise stresses for typical values of r between 0.4 and 0.6.

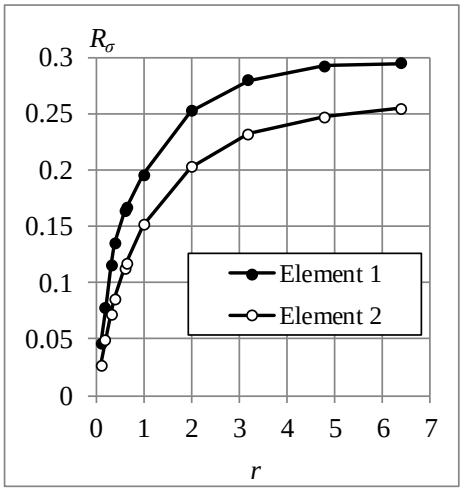

Figure 12 – The influence of chordwise stiffeners area on the ratio R_σ.

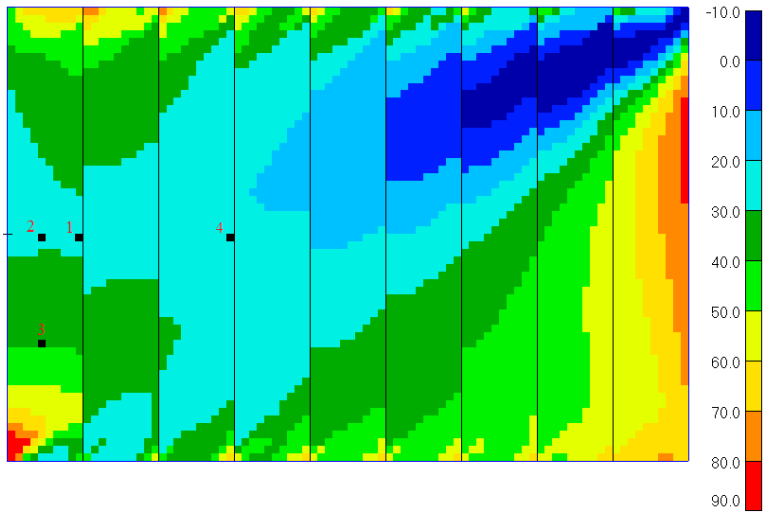

Figure 13 – The chordwise stress distribution for the ply angle of 30°.

In the second case, when the skin is made of composite material, the occurring chordwise stresses can sufficiently influence on ply strength characteristics since the allowable stress in the chord direction is usually significantly less than ones in the span direction. Parametric analyses were performed to determine stress distribution under tension and compression loads at the varying angle of unbalanced ply. In Fig. 13, the stress σ_x distribution is shown at the ply angle $\varphi = 30°$. The maximum values of chordwise stresses take place in the region of applied load and the zones of spar-rib intersection. The dependencies of the parameter R_σ from ply orientation φ for elements 3 and 4 (Fig. 13) are presented in Fig. 14. In addition, the values of R_σ obtained by using analytical model 2 are given. Good agreement between results for the model with chordwise restraints and FE results for element 3, where the medium level of chordwise stresses takes place, is seen in the range of unbalanced ply angles from 0° to 60°.

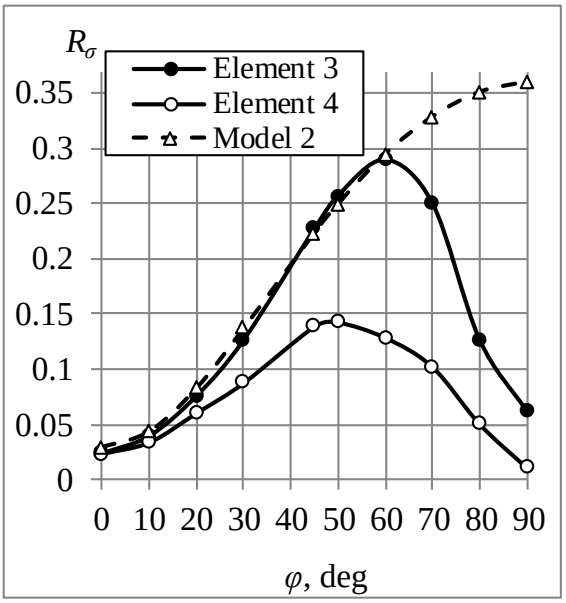

Figure 14 – The dependency of R_σ on ply orientation.

The presence of high stresses in chord direction at ply angles close to zero can lead to a strong decreasing in strength. The dependency of load factors by the Tsai-Hill criterion in element 3 under tension and compression are shown in Fig. 15 at varying ply angle.

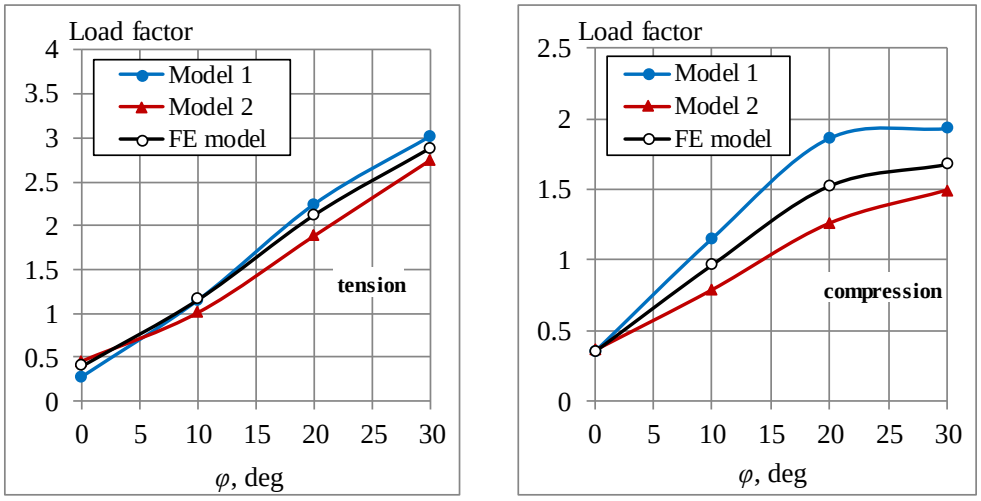

Figure 15 – Load factors in the ply for panel tension and compression.

Note that at the ply angle $\varphi = 0°$ the load factor is 13 % higher for the model with restraints and 30 % lower for the model without restraints than the load factor obtained for the finite element model in the case of tension load. Thus, at design, it is reasonable to use the model 2. FE analyses for typical

chordwise stiffeners yield load factors close to average values obtained for models 1 and 2.

5. Parametric research of stresses near panel stiffener

Consider the problem of determining the stress distribution arising at the tension of panel with a stiffener that restrains deformations in the chordwise direction and causes a non-uniform distribution of chordwise and longitudinal stresses. Since there is no theoretical solution of the problem, the stiffener is modeled by different types of finite elements: 1D (bar), 2D (shell) and 3D (hexahedral) (Fig. 16). The panel length is 1 m, the width – 0.5 m and the thickness – 0.01 m. The parametric research concerns the study of the stiffener cross-section area influence on stress distribution.

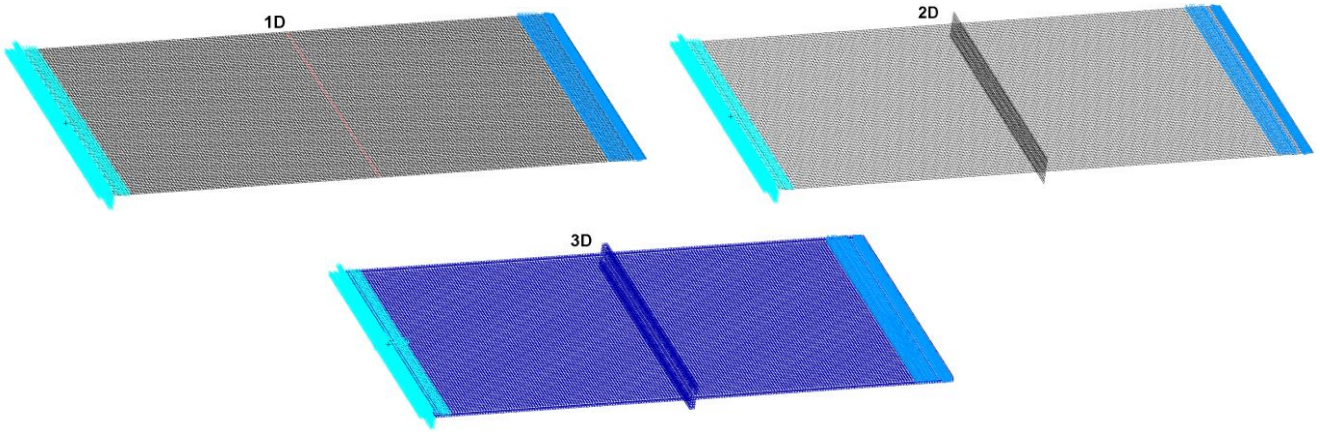

Figure 16 – Different type FE stiffener modeling.

The panel is fixed on one side, and tensile load is applied to another side such that stresses in regular zones are equal to 400 MPa. Fig. 17 represents the longitudinal σ_y (left) and chordwise σ_x (right) stress distributions caused by restrained deformations for the model with a 2D-type FE stiffener (stiffener area of 500 mm^2). Significant growth of longitudinal and chordwise stresses can be seen near the stiffener close to free edges. The stresses σ_x near the stiffener are 10 % of the σ_y stresses. Note that at the increase of stiffener area, the tendency of the chordwise stress growth is observed. The ratio of the maximum chordwise stress to the maximum longitudinal stress depended on the stiffener area is shown in Fig. 18 for different FE types of the stiffener.

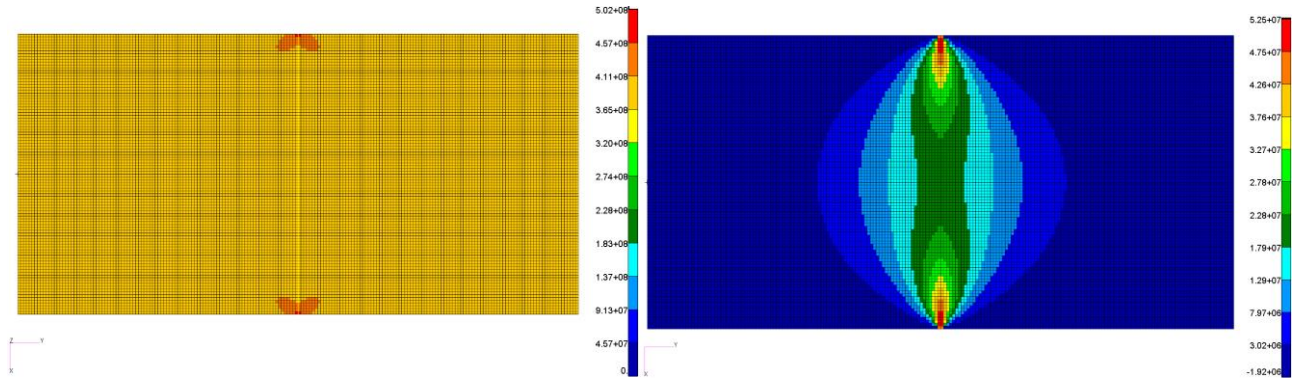

Figure 17 – The distribution of σ_y (left) and σ_x (right) stresses (MPa).

As the strength criterion at the design of isotropic metal structures, the constraints on equivalent von Mises stresses are used. Note that the level of such stresses in the panel is lower than the nominal applied stress near the stiffener, excluding a small zone near the free edge. It is due to the fact that in isotropic panels, the chordwise deformation restraint reduces equivalent stresses. Therefore, in simplified beam models, the disregarding of chordwise stresses gives a conservative estimation of wing panel strength.

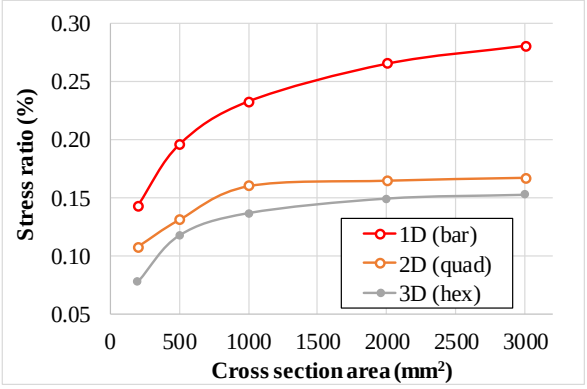

Figure 18 – Chordwise-to-longitudinal stress ratio.

When the composite material is used, the occurring chordwise stresses can significantly influence its strength characteristics, for instance, when calculated by the Tsai-Hill criterion. It is because laminate has sufficiently different allowable stresses in fiber and matrix. The strength of matrix material can be by an order or more lower than strength in the fiber direction. The presence of chordwise stresses in plies can lead to a significant reduction of strength margin. The research was performed for the panel made of composite material with quasi-orthotropic layout 0°[50 %], ±45°[40 %] and 90°[10 %]. In Fig. 19, the ratio σ_x / σ_y is given for each element in laminate (part of the panel with stiffener).

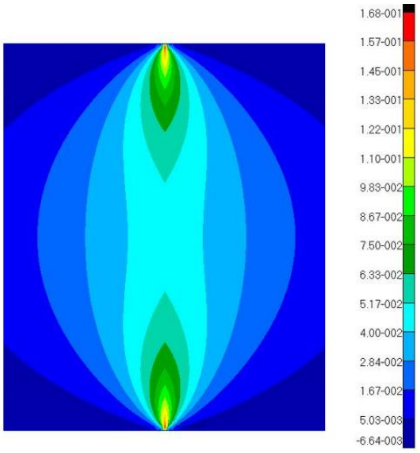

Figure 19 – The ratio σ_x / σ_y for laminate near the stiffener.

Comparison with the metallic panel shows that chordwise stresses are higher and consist of 16.8% of longitudinal ones. There is a correlation between σ_x / σ_y and the ratio σ_2 / σ_1, where σ_1 corresponds to the stress along the fiber direction and σ_2 – the stress in the chordwise direction. Note that the maximum value of σ_2 / σ_1 corresponds to plies with an orientation angle of 90° and is equal to 34%. In ±45° plies, this ratio is 16% and is 1% in plies with an orientation of 0°. At the increase of stiffener cross-section area, the stress concentration zone becomes bigger in the chordwise direction, and the maximum value of σ_2 / σ_1 reaches up to 0.9–1.0 in the 90° ply.

6. Optimization of structures with local stress peculiarities

Stress peculiarities in local zones outlined above should be considered in structural optimization. A thickness change through a whole structure with local stress concentration leads to a significant weight increase, so it is important to develop an approach accounting for local stresses. For understanding in developing an efficient algorithm, the classical optimization problem of a plate with a hole under tension load is considered here. The attempts to enhance the concentration zone by larger thickness and the size of the zone in the radial direction (Fig. 20) lead to the change of maximum equivalent stress localization. They take place beyond the design domain (Fig. 21).

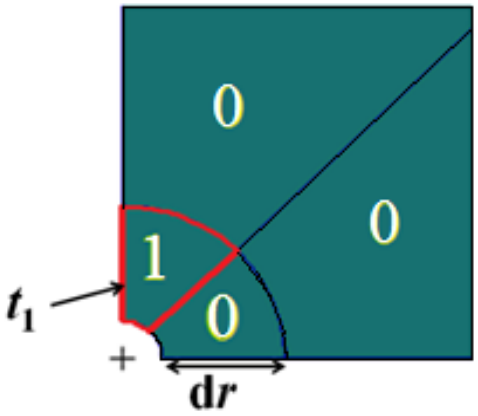

Figure 20 – Design domain.

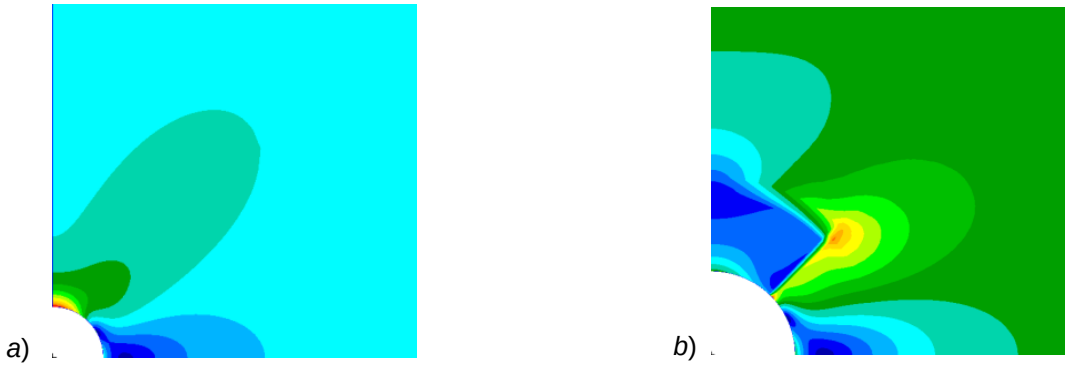

a) *b*)

Figure 21 – Stress distribution before (*a*) and after (*b*) parametric optimization.

Thus, engineering approach based on parametric research is still complicated in determining rational hole edging. Therefore, the optimization algorithm based on the mathematical programming method (method of feasible directions) is used. In Fig. 22(*a*), zones of design variables are shown for one of the design model variants (Fig. 22, *b*). The size of zones is chosen regarding the maximum stress gradient. The meshes of different fidelity are considered. As a constraint, it is assumed that von Mises stress in each element does not exceed 400 MPa. The same tensile stress is applied as a force to the plate boundary.

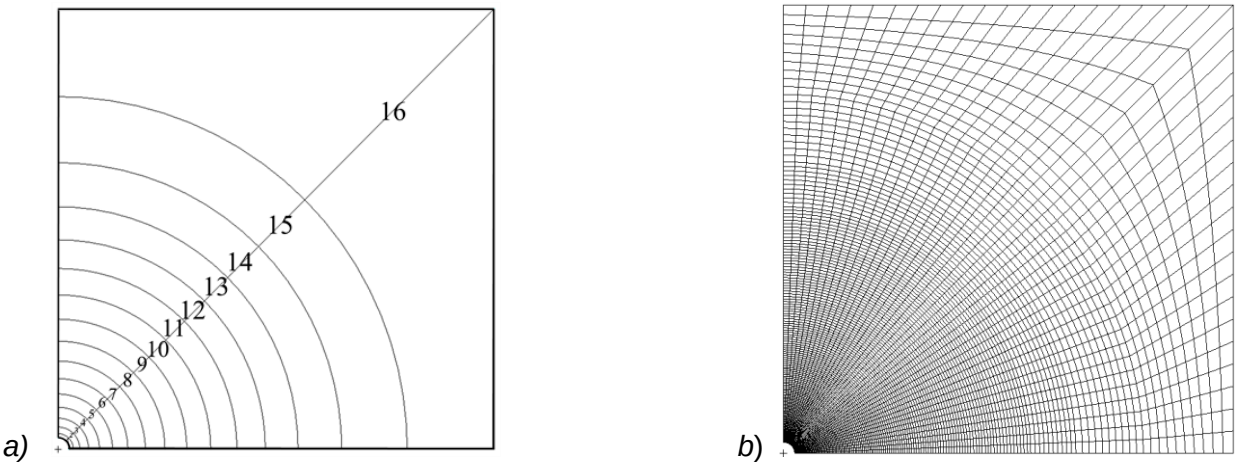

a) *b*)

Figure 22 – Design variable zones (*a*) and FE model (*b*).

In Fig. 23(*a*), the thickness distribution is shown in dependency on distance from the hole center. It can be seen that for a various number of design variables, the thickness distribution is different in zones around the hole though the masses of optimal structures are close. Optimal panel masses for 6, 9 and 19 design variables are 0.619, 0.618 and 0.634, correspondingly. The obtained panel after optimization is modeled by 3D finite elements (hexahedron). The equivalent stress distribution in the optimal panel and the thickness behavior around the hole are presented in Fig. 23(*b*).

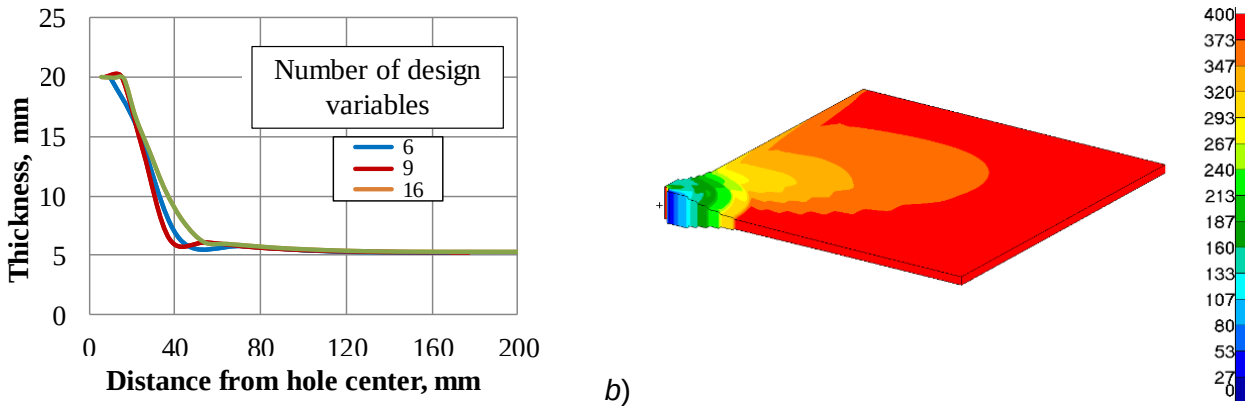

a) *b)*

Figure 23 – Thickness dependency on distance from the hole (*a*) and behavior in 3D model (*b*).

7. Conclusion

Parametric researches were performed on determining local stress distribution near the cross stiffener in the wing panel. It was shown that deformation restraint leads to the non-uniform distribution of stress components, in particular, high-level chordwise stresses occur. It was emphasized that in the case of composite material, it is important to take into consideration chordwise stresses as they drastically influence the strength characteristics of plies. To perform optimization researches including strength, stiffness and aeroelasticity requirements, two simple analytical beam models of a wing-box were developed: with and without restraint deformations. It was outlined that the strength margin should be taken as the maximum value obtained by these models. Models were tested on the example of the wing-box described by the finite element method. Using various ways of modeling, the analysis of stresses and strains was fulfilled for the panel with the hole. The optimization approach was applied to determining the rational hole edging. It was shown that the method of feasible directions allows finding optimal structure with increasing thickness to stress concentration. The veracity of the obtained result is confirmed on the problem in 3D treatment.

8. Contact Author Email Address

mailto: tuktarovsa@mail.ru

9. Copyright Statement

References

[1] Timoshenko S., Gudier J. *Theory of Elasticity*. M.: Nauka, 1979.

[2] Muskhelishvili N. *Some Principal Problems of Mathematical Theory of Elasticity*. M.: Nauka, 1966.

[3] Tuktarov S., Chedrik V. Some Aspects of Composite Wing-Box Modelling by Anisotropic Beam. *Ucheniye zapiski TsAGI*, T. XLVI, No. 3, pp 70–81, 2015.

[4] Weisshaar T., Foist B. Vibration Tailoring of Advanced Composite Lifting Surfaces. *J. Aircraft*, Vol. 22, No. 2, pp 141–147, 1985.

[5] Chedrik V., Kagan I. Method of Lifting Surface Design With the Use of Composite and Metal Materials. *Tekhnika Vozdushnovo* Flota. T. LXXVII, No. 5-6 (664-665), pp 86-94, 2003.

[6] Jones R. *Mechanics of Composite Materials*. McGraw-Hill Book Company, 1975.